2014 Second International Conference on 3D Vision

A Structure from Motion Approach for the Analysis of Adhesions in Rotating Vessels

Patrick Waibel, Jörg Matthes, Lutz Gröll, Hubert B. Keller
Institute for Applied Computer Science
Karlsruhe Institute of Technology (KIT)
Hermann-von-Helmholtz-Platz 1, 76344 Eggenstein-Leopoldshafen
Email: patrick.waibel@kit.edu

***Abstract*—While processing material in rotating vessels such as rotary kilns, adhesions on the inner vessel wall can occur. Large adhesions usually affect the process negatively and need to be prevented. An online detection and analysis of adhesions inside the vessel during operation could allow the process control to deploy counter-measures that prevent additional adhesions or reduce the adhesion's sizes. In this paper, we present a new method that enables an image-based online detection, tracking and characterization of adhesions inside a rotating vessel. Our algorithm makes use of the rotational movements of adhesions in a structure from motion approach which allows for the measurement of the positions and heights of adhesions with a single camera. The applicability of our method is shown by means of image sequences from a rotating vessel model as well as from an industrially used cement rotary kiln.**

***Keywords*-structure from motion, 3D reconstruction, rotary kiln, rotating vessel, adhesion**

I. Introduction

Rotating vessels are widely used to process materials in chemical plants. They usually have a cylindrical shape and their rotation axis is slightly inclined to the horizontal. The raw material for processing is fed into the vessel at its upper end. While the raw material is mixed by the rotary motion of the vessel it gradually moves towards the vessels lower end.

Typical representatives of industrially used rotating vessels are rotary kilns which are employed for cement production, metal recycling or waste incineration [1], [2]. A common problem during the operation of rotary kilns are adhesions (cakings) of the processed material on the inner vessel wall. Up to a small height, adhesions are sometimes intended in order to build up a protective layer for the inner vessel wall. Nevertheless, an increased adhesion formation is problematic. Large adhesions usually have a negative influence on the process behavior by provoking worse mixing or changed flow conditions. They can even lead to an accretion of the entire cross-section of the vessel. In this case, a complete shutdown of the plant has to be induced in order to remove the adhesions.

An online detection of the height and position of adhesions inside the vessel could prevent further adhesions or degenerate existing adhesions via an appropriate change of process parameters e.g. via adaptions of the temperature profile, the material composition or the feed charge. Current methods to analyze adhesions use infrared line scanners that examine the outer wall of the rotating vessels with respect to temperature variations. This approach only works when there are differences between the vessel's inside temperature and the outside temperature and additionally presumes a known temperature profile inside the vessel. Due to the thickness of the wall, inferring single adhesions from the temperature distribution of the vessel's outer wall is often not possible.

In the past few years custom-built camera systems have been used to observe the inside of rotary kilns from the back or front opening for monitoring purposes. The so acquired images offer the chance to analyze the processed material [3] or the employed burner systems [4], [5]. Moreover, adhesions inside the vessel can be observed in the images. Nevertheless, an automatic image-based detection and analysis of adhesions does not exist so far.

In this paper, we present a new method that allows for the automatic image-based analysis of adhesions inside rotating vessels via a structure from motion approach. This newly extracted information can be used to build up an approximate elevation profile of the inner vessel wall. In Figure 1 a schematic representation of the analyzed scenario is given. It should be mentioned that the presented method is not a classical structure from motion approach since the camera position is fixed and specific constraints of the scenario are considered.

The underlying task of the proposed method can be formulated as follows: Let at least three images at various succeeding points in time acquired by a stationary camera observing the inside of the rotating vessel with at least one adhesion be given. Additionally, the employed camera is not located on the rotational axis of the vessel. Then, the height and the position of the adhesions inside the vessel are to extract from the acquired images.

In order to improve the readability of this paper the following simplifications are conducted:

- The rotating vessel is of a cylindrical shape.
- The rotating movements of the adhesions in the kiln

978-1-4799-7000-1/14 $31.00 © 2014 IEEE
DOI 10.1109/3DV.2014.38

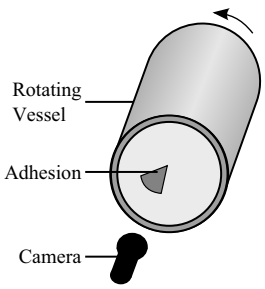

Figure 1. Schematic representation of the scenario.

correspond to circles in the images.

The extension to the more general case of arbitrary-shaped vessels and oval or elliptic movements are addressed in Section V.

A. Paper Outline

The remainder of the paper is organized as follows. In Section II the problem formulation is depicted in general. Mathematical relationships between image data and real-world dimensions are presented in Section III. Section IV covers implementation details from the image feature detection to the extraction of the adhesion's positions and heights. A discussion of extensions to the proposed method are given in Section V. In Section VI some results of our method applied to a rotating vessel model as well as to an industrial rotary kiln for the cement production are shown.

B. Notation

In this paper we use the following notation. Vectors are denoted by lowercase bold letters such as $\boldsymbol{a}, \boldsymbol{b}, \boldsymbol{c}$. Scalars are denoted by lowercase Roman or Greek letters (e.g. a, b, α). All vectors are assumed to be column vectors, if not stated otherwise. A superscript T denotes a transposition.

II. Problem Formulation

The main idea behind the presented method is to make use of the specific circular movement that an adhesion inside a rotating vessel describes in an image sequence. This information shall be used to determine the depth and the height of that adhesion inside the rotating vessel.

In order to compare the paths of different interest points in the vessel two snapshot situations of the vessel are depicted and merged in one figure. Especially, we are interested in points representing the top of an adhesion (symbolized by a triangle) and points on the inner wall. The first snapshot is taken when the examined points are at $0°$ and the second snapshot when they are at $180°$. This configuration is shown in Figure 2 for different scenarios.

In a first scenario one adhesion is analyzed with a camera position which is shifted to the rotational axis. Figure 2a shows a comparison of circular paths, between a point $\boldsymbol{p}_1$ on top of the adhesion and a point $\boldsymbol{p}_2$ representing a point

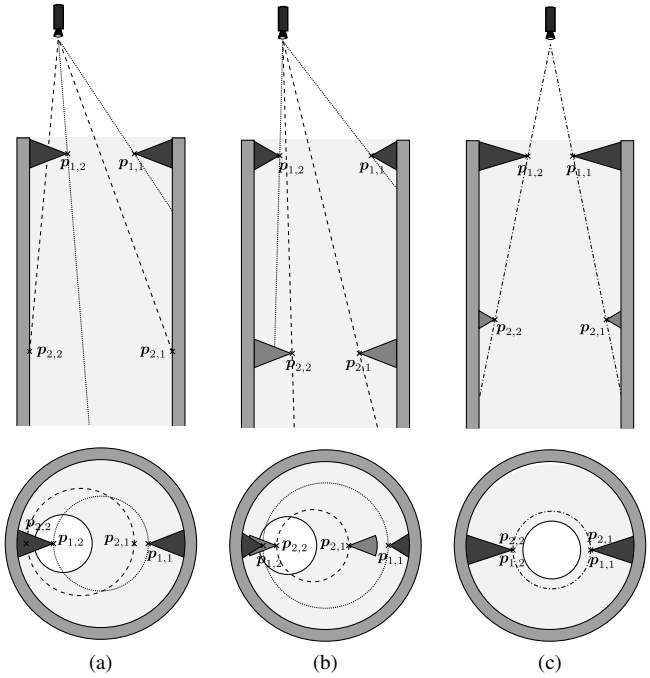

Figure 2. Top-views of a rotating vessel in the level of the rotation axis with a camera (top). Schematic camera images of the same situation (bottom). Points $\boldsymbol{p}_{1,1}$, $\boldsymbol{p}_{1,2}$ as well as $\boldsymbol{p}_{2,1}$ and $\boldsymbol{p}_{2,2}$ represent the same points after half a revolution of the vessel. Point $\boldsymbol{p}_1$ depicts the peak of an adhesion which is close to the front of the vessel and the camera, whereas point $\boldsymbol{p}_2$ represents a peak of another adhesion respectively a point on the inner wall located more distant from the camera.

on the inner wall. The second index of the points $\boldsymbol{p}_1$ and $\boldsymbol{p}_2$ denotes the particular snapshot. At the two intersection points of the circles both points are at the same position in the image. It can be seen, that the circle of point $\boldsymbol{p}_1$ has a smaller radius than the one of point $\boldsymbol{p}_2$ and that its center is located closer to the center of the front of the vessel.

In the second scenario (Figure 2b) another slightly larger adhesion is located behind the first adhesion. In this case, the circle of point $\boldsymbol{p}_1$ (first adhesion) has a larger radius as the one of point $\boldsymbol{p}_2$ (second adhesion). Just like in scenario 1, the center of the first adhesions's circle is located closer the center of the front of the vessel.

Considering these properties, it can be assumed that the positions of the circle's centers represent the depth of the adhesion inside the vessel in some way. Besides, a relationship between the radius and the height of the adhesion can be expected.

In the third scenario (Figure 2c) the camera position is located on the rotational axis of the vessel. Here, all possible circular paths of adhesions as well as points on the vessel wall possess the same rotation center in the images. In this case a deduction of the depth inside the vessel by examining the rotation center is not feasible.

Based on these observations, it is obvious that all possible

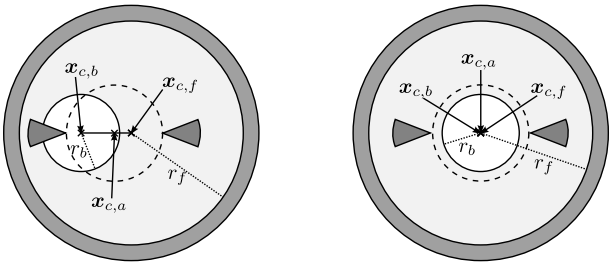

(a) Shifted Position (b) Centered Position

Figure 3. Comparison of two camera positions. Rotation centers of the front side of the vessel $\boldsymbol{x}_{c,f}$, of the back side $\boldsymbol{x}_{c,b}$ and of an adhesion $\boldsymbol{x}_{c,a}$ are outlined.

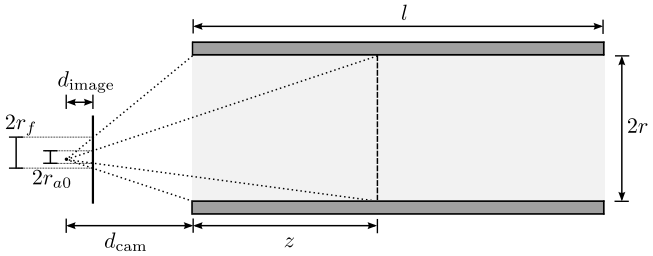

Figure 4. Top-view of a rotating vessel in the level of the rotation axis. Assuming a pinhole camera, the image plane, relevant optical paths and sizes are given in order to outline the relationship between depth in the vessel and the image-based radius when no adhesions in the vessel appear.

rotation centers of adhesions have to be located on a line segment which is bounded by the rotation center $\boldsymbol{x}_{c,f} = \left[x_{c,f}, y_{c,f}\right]^T$ of the front end of the vessel and the rotation center $\boldsymbol{x}_{c,b} = \left[x_{c,b}, y_{c,b}\right]^T$ of the back end (Figure 3a). In the case of a centered camera position, all centers fall together in one point (Figure 3b).

Besides the depth, the angular position of an adhesion is required to complement the position information. Since this can be accomplished straightforwardly by simply using a reference point this issue will not further be addressed in this paper.

In the following section, the found relationships between image-based information and real world information are further examined. Formulas are given that provide the possibility to derive the adhesions heights and depths inside the vessel solely by analyzing their circular paths in the images.

III. Method

It it essential to find a proper mathematical connection between image coordinates and real-world dimensions to build up an image-based adhesion analyzing. In Lemma 1 the relationship between the rotation center in the image and the depth inside the vessel is depicted. Lemma 2 provides a possibility to derive the adhesion's height from its image-based rotation center and radius.

Lemma 1. *The relationship between the x-image-coordinate of an adhesions's rotation center $x_{c,a}$ and the depth z of the adhesion inside the vessel is given by*

$$z = \frac{l}{\frac{r_f}{r_b} - 1} \left(\frac{r_f}{\left(\frac{x_{c,a} - x_{c,b}}{x_{c,f} - x_{c,b}}\right)(r_f - r_b) + r_b} - 1 \right). \quad (1)$$

The same value z occurs if the y-image-coordinate is used:

$$z = \frac{l}{\frac{r_f}{r_b} - 1} \left(\frac{r_f}{\left(\frac{y_{c,a} - y_{c,b}}{y_{c,f} - y_{c,b}}\right)(r_f - r_b) + r_b} - 1 \right) \quad (2)$$

Proof: From Figure 4 the following geometrical relationships between the distance d_{image} of the image plane, the distance d_{cam} between the camera and the front side of the vessel, the depth inside the vessel z, the vessel length l, the vessel radius r, the image-based radius of the front side of the vessel r_f and the image-based radius r_{a0} of a point on the vessel wall in depth z can be deduced applying the intercept theorem,

$$\frac{d_{\text{image}}}{d_{\text{cam}} + z} = \frac{r_{a0}}{r}. \quad (3)$$

Further

$$\frac{d_{\text{image}}}{d_{\text{cam}}} = \frac{r_f}{r} \quad (4)$$

holds. Considering $z = l$ which corresponds to $r_{a0} = r_b$, where r_b is the image-based radius of the back side of the vessel, results in

$$\frac{d_{\text{image}}}{d_{\text{cam}} + l} = \frac{r_b}{r}. \quad (5)$$

Using (4) and (5) to substitute d_{cam} and d_{image}, (3) can be written as

$$r_{a0} = \frac{r_f}{1 + \frac{z}{l}\left(\frac{r_f}{r_b} - 1\right)}. \quad (6)$$

Equation (6) solved for the depth z subject to the radius r_{a0} gives

$$z = \frac{l}{\frac{r_f}{r_b} - 1}\left(\frac{r_f}{r_{a0}} - 1\right). \quad (7)$$

Figure 5 depicts the relationship between the radius and the rotation center. Obviously, the closer the rotation center is located to the vessel front, the larger the radius gets. Applying the intercept theorem for segments on parallels the relation

$$\frac{\overline{AB}}{\overline{DE}} = \frac{\overline{BC}}{\overline{EF}} \quad (8)$$

can be deduced. Expressing the above segments with the radii and x-coordinates of the centers

$$\frac{x_{c,a0} - x_{c,b}}{x_{c,f} - x_{c,b}} = \frac{r_{a0} - r_b}{r_f - r_b} \quad (9)$$

and using the y-coordinate of the centers

$$\frac{y_{c,a0} - y_{c,b}}{y_{c,f} - y_{c,b}} = \frac{r_{a0} - r_b}{r_f - r_b}. \quad (10)$$

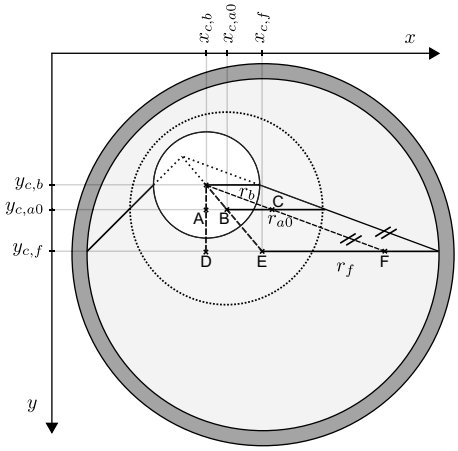

Figure 5. Schematic camera-image of the frontal view of a rotating vessel. Geometric relationships between rotation centers and their corresponding radii are outlined.

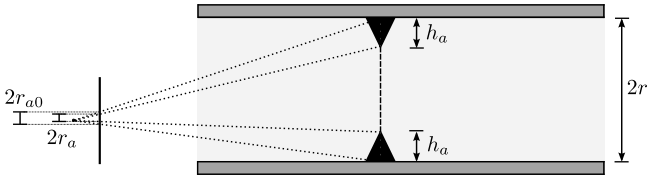

Figure 6. Top-view of a rotating vessel in the level of the rotation axis. Assuming a pinhole camera, the image plane, relevant optical paths and sizes are given in order to outline the relationship between the height of an adhesion and the image-based radii.

holds. Substituting r_{a0} in (7) using (9) and (10) leads to (1) and (2). ■

The next Lemma considers the relationship between the image-based radius and rotation center of an adhesion and its height in real-world dimensions.

Lemma 2. *The height h_a of an adhesion subject to the image-based radius of its peak r_a and its rotation center x-coordinate $x_{c,a}$ is given by*

$$h_a(x_{c,a}, r_a) = r\left(1 - \frac{r_a}{\left(\frac{x_{c,a}-x_{c,b}}{x_{c,f}-x_{c,b}}\right)(r_f - r_b) + r_b}\right) \quad (11)$$

respectively

$$h_a(y_{c,a}, r_a) = r\left(1 - \frac{r_a}{\left(\frac{y_{c,a}-y_{c,b}}{y_{c,f}-y_{c,b}}\right)(r_f - r_b) + r_b}\right) \quad (12)$$

by using the y-coordinate of the rotation center $y_{c,a}$.

Proof: In Figure 6 the following relationship can be seen by employing the intercept theorem,

$$\frac{r - h_a}{r} = \frac{r_a}{r_{a0}}. \quad (13)$$

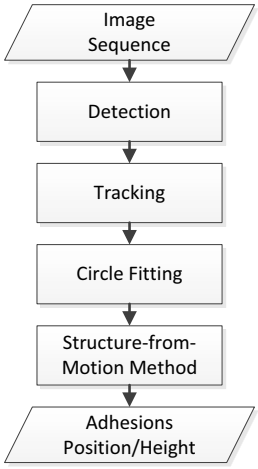

Figure 7. Image processing chain

Solving (13) for h_a yields

$$h_a = r\left(1 - \frac{r_a}{r_{a0}}\right). \quad (14)$$

Substituting r_{a0} using (9) and (10) as well as employing the relations $x_{c,a} = x_{c,a0}$ and $y_{c,a} = y_{c,a0}$ (the rotation center is independent from the height of an adhesion) results in (11) and (12). ■

IV. Implementation

The entire processing chain for the extraction of adhesion heights and depths after acquiring an image sequence of the vessel's inside comprises several processing steps (Figure 7). The single steps are explained in the following subsections.

In practice, the geometric model of the vessel is usually known beforehand and so is the camera position. This means, the vessel's radius and length, as well as the vessel's front and back side's rotation centers in the images are given parameters.

A. Detection

The first step of the processing chain is the detection of relevant local image points. Relevant image points are primarily adhesion peaks but not exclusively since the more points are used the more detailed an elevation profile of the inner vessel becomes. The choice of the detector algorithm depends on the particular application. Varying process conditions can complicate the detection of the same interest point in subsequent image frames. Possible proven methods to identify relevant local interest points in an image are the Speeded Up Robust Features (SURF) algorithm [6] or the Features from Accelerated Segment Test (FAST) algorithm [7], [8]. The region of interest, which is used for the detection algorithm, is given by the image part that comprises the inside of the vessel.

B. Tracking

Tracking requires a method that extracts descriptors of the interest points that are rotational invariant and allow for a reliable matching of the interest points in subsequent images. In our case, we use Fast Retina Keypoint (FREAK) descriptors [9] to perform the matching of the interest points between two images.

To further improve the assignment of the detected interest points a Kalman filter for each new interest point sequence is initialized. The Kalman tracking filter allows for the prediction of the position of the interest point in subsequent frames and the consideration of missed detections in single frames. We use the predicted positions as centers of small circular regions of interests (ROIs) where the possible interest points matches have to be located. Detected interest points that are outside of these ROIs are not taken into account for the specific matching. In order to keep up a linear movement, which is a requirement for the Kalman tracking filter, the Cartesian coordinates are converted to polar coordinates. As long as the actual rotation center of the interest point is unknown (i.e. before the circle fitting) the middle of the line segment representing all possible rotation centers is used for the conversion. Once the circle fitting took place, the according circle center is applied.

C. Circle Fitting

In this processing step the circle parameters *radius* and *center* of each adhesion are estimated from the detected image positions. Fitting of circles to given data points is a common computer vision task which involves e.g. the minimization of the sum of squares of the geometric distances via

$$E_{\text{geom.}} = \sum_{k=1}^{N_p} \left(\|\boldsymbol{p}_k - \boldsymbol{x}_c\|_2 - r \right)^2 \rightarrow \min . \qquad (15)$$

Here, the number of the data points $\boldsymbol{p}_k$ is given by N_p and the corresponding radius is represented by r. For employing a circle fitting at least three positions of the observed adhesion have to be known. The required number of image positions depends on the degrees of freedom which is three for a circle fitting and would e.g. be higher for an ellipse fitting approach. In our application we have additional prior knowledge which on the one hand can be used to reduce the degrees of freedom of the fitting task and on the other hand improves the fitting accuracy. This prior knowledge is given by the constraint that all possible rotation centers of adhesions have to be located on the line segment bounded by the rotation center of the vessel's front end and the rotation center of the back end (see Section II). The adaption to a circle fitting problem can be done easily by substituting one center variable with the help of the line equation

$$y_c = \frac{y_{b,c} - y_{f,c}}{x_{b,c} - x_{f,c}} x_c + y_{b,c} - \frac{y_{b,c} - y_{f,c}}{x_{b,c} - x_{f,c}} x_{b,c}. \qquad (16)$$

The output of the circle fitting step is a list that contains the radius and center of each adhesion.

D. Structure from Motion Method

In this step, the calculations presented in Section III are conducted for each tracked adhesion point. The aim of this processing step is to connect the 2D-image-based motion information to 3D-real-world structure information. That means, after determining the particular circle parameters the corresponding depths and heights of the adhesions inside the vessel are calculated. Given this information, an elevation profile of the inner vessel wall can be built up. Due to occlusions caused by large adhesions or missed detections a complete elevation profile is usually not possible.

V. Extensions

Up to now some simplifying presumptions concerning the vessel and the imaging were made. In the following, extensions of the method are proposed.

A. Arbitrary-shaped Rotating Vessels

The presented method is also applicable for more general shapes of the vessel. Two restrictions have yet to be made to ensure a correct determination of real-world information from the image data:

- the rotational axis is orthogonal to the base of the vessel
- the cross-section of the vessel is identical along the rotational axis

In the more general case, it is indispensable to consider the rotational angular position α of the adhesion since the cross-section of the vessel is not invariant to rotation. Instead for radii, distances d from the rotation center have to be accounted for. This leads to adaptions in the equations proposed in Lemma 1 and Lemma 2, where the following substitutions have to be done: $r_a \triangleq d_a(\alpha)$, $r_b \triangleq d_b(\alpha)$, $r_f \triangleq d_f(\alpha)$, $r_{a0} \triangleq d_{a0}(\alpha)$ and $r \triangleq d(\alpha)$.

B. Non-circular Paths

In the previous sections we assumed that the rotational movements of adhesions are reflected by circular paths in the images. Actually, the movements correspond to oval paths in the images where the ratio of the oval's axes depend on the distance of the camera from the rotational axis of the vessel. Therefore, the employed simplification is not applicable to camera positions highly shifted from the rotational axis of the vessel. Since the mathematical handling of ovals is rather complex a convenient way is the implementation of an ellipse fitting approach in these cases. Algorithms that allow for the fitting of ellipses to given data points are e.g. described in [10], [11] and [12].

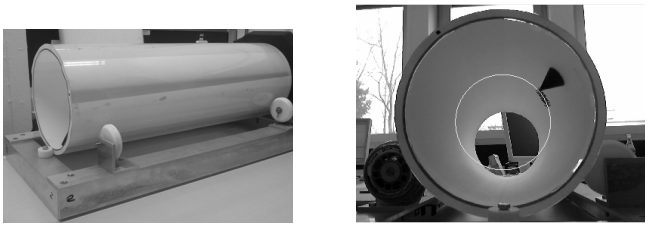

(a) (b)

Figure 8. Experimental setup of a rotating vessel (a) with detection and tracking points of adhesion dummy with height 30 mm and depth 100 mm in acquired image (b).

C. Miscellaenous

In some situations the detection of the upper end of the vessel in the image sequences is not possible e.g. due to bad visibility conditions caused by a high particle load in the vessel atmosphere. In this case, it is also feasible to use other reference points in known depths of the vessel to build up the geometric model.

VI. Results and Discussion

In industrial vessels it is hardly possible to validate the measured data of adhesions while the vessel is in operation (e.g. due to high temperatures). Hence, we built up an experimental setup of a rotating vessel model that allows for the comparison of measured data with ground truth data in order to validate our method. The principal applicability of our method under industrial conditions is shown on the basis of image data acquired at a rotary kiln for the cement production.

A. Experimental Setup

The experimental setup consists of a vessel with a length of 0.6 m and a radius of 0.09 m. Its rotation speed can be manually adjusted. We deployed black cones of different sizes that can be placed inside the vessel to simulate the adhesions. Using a marker at the frontal vessel wall allows for the determination of angular positions of the adhesions. The employed camera has a resolution of 960×1280 pixels. Here, we used the FAST interest point detector to locate the adhesion peaks.

Figure 8 shows the experimental setup and the tracked detection points of one adhesion dummy in an acquired image. In Table I a comparison of the estimated values for adhesion heights and depths with our proposed method and the real values are given for three different experiments. The estimated adhesion heights and depths are the calculated values after half a revolution of the vessel. Based on these values the relative error is determined.

In all experiments the estimated depth and height values approximate the real values with low errors. More precise values are expected by employing cameras with higher image resolutions.

Table I
Comparison of estimated image-based adhesion data and real values in experimental setup (H:height, D:depth; unit: mm)

	Exp.1		Exp.2		Exp.3	
	H	D	H	D	H	D
Image-based	30.7	77.6	20.5	48.2	28.9	101.1
Real value	30.0	80.0	20.0	50.0	30.0	100.0
Relative error	2.3%	3.0%	2.5%	3.6%	3.7%	1.1%

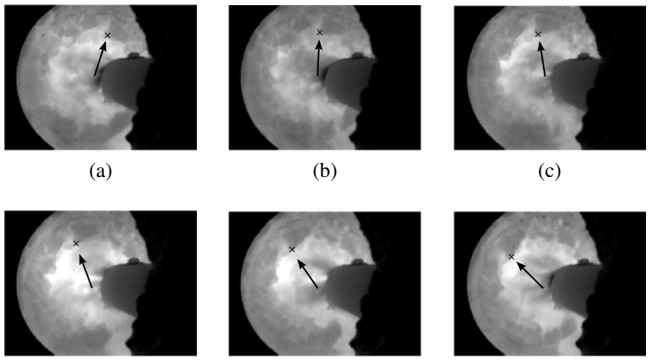

(a) (b) (c)

(d) (e) (f)

Figure 9. Image sequence of rotary kiln for cement production with marked adhesion at the inner wall.

B. Rotary Kiln for Cement Production

Figure 9 shows an image sequence of a rotary kiln which is used for the cement production. In the analyzed situation numerous adhesions at the kiln's inner wall are noticeable. One distinct large adhesion is marked in the images. The image data was acquired with a custom-built infrared camera with air supply and water cooling. The camera's resolution is 320×240 pixels. Due to the high prices of such camera systems, stereo vision to gather 3D information of the kiln's inside is no option. In Figure 10 the circle of the vessel's front side, a reference circle in a known depth of the kiln (back side circle) as well as the line of possible rotation centers are drawn. Additionally, the estimated circle of the adhesion's movement is given.

Using the given parameters (Table II) our method provides an estimated height of 0.51 m and a depth inside the kiln of 0.4 m for the analyzed adhesion. Both values are plausible for the given situation in the rotary kiln. Due to the harsh environmental conditions inside the rotary kiln (e.g. dust clouds, varying illumination) the detection part of the proposed method was conducted manually in this case. Future improvements of our method comprise the increase of the robustness of the detection part at highly challenging conditions.

Both applications show the feasibility of our structure from motion method for the analysis of adhesions inside rotating vessels. Nevertheless, for applying the entire image processing chain from Figure 7 it is required that relevant image points (especially adhesion peaks) can be detected

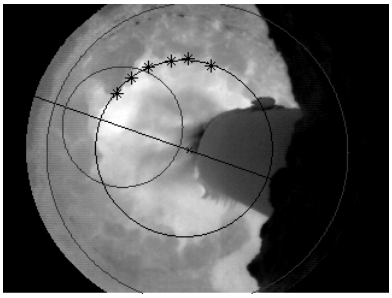

Figure 10. Geometric data of a rotary kiln for the cement production.

Table II
PARAMETERS OF THE FRONT SIDE AND A REFERENCE CIRCLE IN A KNOWN DEPTH (BACK SIDE CIRCLE) FOR THE CEMENT ROTARY KILN IMAGE SEQUENCE.

Front side circle	$x_{c,f} = 162$ $y_{c,f} = 124$ $r_f = 125$
Back side circle	$x_{m,b} = 100$ $y_{m,b} = 103$ $r_b = 50$
Depth back side circle	$l = 5\,m$
Radius vessel	$r = 1.5\,m$

and tracked in a robust way. In particular inside industrially used vessels, disturbances such as flames, smoke or flue ash can occur. Consequences are varying illumination conditions or occlusions which lead to difficulties in the detection and tracking step. Due to possible high particle loads inside a vessel the transmission could also be low and thereby limit the maximum depth where adhesions can be detected. Another limiting factor is the image resolution which determines the preciseness of measurements. At low image resolution which are e.g. still common in currently available cameras for rotary kilns, this can be a limiting factor for the image-based analysis of adhesions deep inside the vessel.

VII. CONCLUSION

The presented structure from motion based method opens the new possibility to analyze adhesions inside rotating vessels with regard to their positions and heights by means of computer vision. Using the motion information of adhesions in the acquired image sequences it is possible to deduce on the adhesions' positions and heights with a single camera. The applicability of the method was shown by using image sequences from an experimental setup as well as from an industrial cement rotary kiln. The proposed method allows for a deeper insight in the process behavior of industrially used rotating vessels such as rotary kilns. The extracted information can be used to optimize the process control in order to avoid critical adhesions inside rotating vessels. Future works comprise improvements in the detection and tracking part especially for demanding industrial environments and the implementation of an ellipse fitting approach.

REFERENCES

[1] A. A. Boateng, *Rotary Kilns: Transport Phenomena and Transport Processes*. Butterworth-Heinemann, 2008, vol. 1.

[2] J. Matthes, P. Waibel, and H. B. Keller, "A new infrared camera-based technology for the optimization of the waelz process for zinc recycling," *Minerals Engineering*, vol. 24, no. 8, pp. 944–949, 2011.

[3] P. Waibel, J. Matthes, and H. B. Keller, "Segmentation of the solid bed in infrared image sequences of rotary kilns," in *Proc. 7th Int. Conf. on Informatics in Control, Automation and Robotics (ICINCO)*, Jun. 2010, pp. 217–220.

[4] J. Ballester and T. Garcia-Armingol, "Diagnostic techniques for the monitoring and control of practical flames," *Progress in Energy and Combustion Science*, vol. 36, no. 4, pp. 375–411, 2010.

[5] H.-l. Zhang, Z. Zou, J. Li, and X.-T. Chen, "Flame image recognition of alumina rotary kiln by artificial neural network and support vector machine methods," *Journal of Central South University of Technology*, vol. 15, pp. 39–43, 2008.

[6] H. Bay, A. Ess, T. Tuytelaars, and L. Van Gool, "Speeded-up robust features (SURF)," *Comput. Vis. Image Underst.*, vol. 110, no. 3, pp. 346–359, Jun. 2008.

[7] E. Rosten and T. Drummond, "Fusing points and lines for high performance tracking," in *Tenth IEEE Int. Conf. on Computer Vision*, 2005.

[8] ——, "Machine learning for high-speed corner detection," in *Computer Vision – ECCV 2006*, ser. Lecture Notes in Computer Science, A. Leonardis, H. Bischof, and A. Pinz, Eds., vol. 3951. Springer Berlin Heidelberg, 2006, pp. 430–443.

[9] A. Alahi, R. Ortiz, and P. Vandergheynst, "FREAK: Fast retina keypoint," in *IEEE Conf. on Computer Vision and Pattern Recognition*, 2012.

[10] A. Fitzgibbon, M. Pilu, and R. B. Fisher, "Direct least-squares fitting of ellipses," *IEEE Trans. Pattern Anal. Mach. Intell.*, vol. 21, pp. 476–480, May 1999.

[11] Z. Szpak, W. Chojnacki, and A. van den Hengel, "Guaranteed ellipse fitting with the sampson distance," in *Computer Vision ECCV 2012*, ser. Lecture Notes in Computer Science, A. Fitzgibbon, S. Lazebnik, P. Perona, Y. Sato, and C. Schmid, Eds. Springer Berlin Heidelberg, 2012, vol. 7576, pp. 87–100.

[12] K. Kanatani and P. Rangarajan, "Hyper least squares fitting of circles and ellipses," *Comput. Stat. Data Anal.*, vol. 55, no. 6, pp. 2197–2208, Jun. 2011.